

Article

Influence of Salinity and Pb on the Precipitation of Zn in a Model System

Kai Tandon *, Melanie John, Soraya Heuss-Aßbichler and Valentin Schaller

Department of Earth and Environmental Sciences, Ludwig-Maximilians-Universität München, Theresienstr. 41, 80333 Munich, Germany; Melanie@john-stadler.de (M.J.); soraya@min.uni-muenchen.de (S.H.-A.); valentin.schaller@kabelmail.de (V.S.)

* Correspondence: kai.tandon@min.uni-muenchen.com; Tel.: +49-89-2180-4271

Received: 19 December 2017; Accepted: 22 January 2018; Published: 26 January 2018

Abstract: Fly ash from solid waste incineration plants is a source of a significant mass flow of Zn- and Pb-containing waste. Acidic leaching removes most heavy metals from fly ash, but leads to high concentrations of soluble salts in the solution, resulting in a saline solution enriched in heavy metals. Common treatment methods cause voluminous sludge that is mostly disposed of as hazardous waste and hence leads to a loss of Zn and other heavy metals. On a laboratory scale, precipitation experiments with 2000 mg/L Zn were performed to investigate the impact of salinity (0 to >70,000 mg/L Cl, 0 to 5400 mg/L SO₄) and Pb concentration (0 to 800 mg/L) on the formation of mineral phases. The removal efficiency of Zn and Pb after alkalization of the solution was studied. Characterization of the precipitates showed that salinity has a significant impact on the phases produced. At a low salt concentration, zincite (ZnO) is formed. With increasing salinity, the higher concentration of chloride and sulfate increases the stability of various Zn sulphate hydroxides. At a medium salinity of 7000 mg/L, bechererite is predominantly formed, whereas a higher salinity leads to the formation of gordaite. Addition of low amounts of Pb enlarges the stability field of zincite to medium saline solutions but causes lower removal efficiency. The lower removal efficiency observed at low salinity increases at a higher salinity. In high saline solutions, high Pb concentrations (800 mg/L) are needed to form laurionite, a Pb-hydroxychloride phase.

Keywords: water treatment; zinc; lead; zincite; bechererite; namuwite; gordaite; saline solution; brine; waste incineration residues

1. Introduction

Zn is an essential element for living organisms, and a deficiency has a negative impact on the biological function of organisms. However, high concentrations of Zn are harmful to health, causing vomiting, sickness, and diarrhea [1]. Zn is also the fourth-most common metal in use. It is applied in enameling and coating processes, in construction work, or is used in batteries and medicine, to name a few branches. Manifold industries produce wastewater that is enriched in heavy metals, such as Zn. Every year, large amounts of wastewater with a high Zn concentration accrue in industrial sectors such as metalworking, -processing, -finishing, and electroplating. The main use of Pb, for example, is in various industrial branches for the production of batteries, radiation shielding, and electrodes [2]. In contrast, Pb is non-essential and can be harmful even in low concentrations, and therefore should be avoided in the environment. High concentrations of inorganic Pb in the human body can cause anemia, diarrhea, or can induce coma as well as being carcinogenic, mutagenic, and toxic for reproduction [1,3]. Although there are various methods to treat heavy-metal-bearing wastewater, Fu and Wang [4] rate environmental pollution with heavy metals as one of the most severe issues today. Depending on the concentration, methods such as chemical precipitation, adsorption, ion exchange, or membrane filtration are used to remove heavy metals, e.g., Zn. Common methods to treat wastewater polluted

with heavy metals are ion exchange or adding lime milk [5]. The neutralization reaction with $\text{Ca}(\text{OH})_2$ is one of the most utilized methods, but it causes voluminous, heavy-metals-loaded hydroxide sludge. Generally, this slurry is treated physico-chemically and stabilized before deposition. Dissipation of Zn and Pb is the result.

Residues of solid waste incineration, including bottom ash and fly ash, cause a significant mass flow enriched in heavy metals. In general, fly ash (FA) is classified as a hazardous waste due to the high content of leachable heavy metals [6]. Usually, FA is stabilized and disposed in hazardous waste landfills to prevent a release of toxic elements into the environment [6,7]. In this case, Zn, Pb, and other heavy metals are lost from circular economy. At the same time, FA is especially enriched in Zn and, depending on the waste input, also contains many other volatile elements, such as Pb, Cu, Hg, Cd, Cr, As, and Ni [8–10]. Zacco et al. [8] assessed FA as the world's fifth-largest material resource.

There are several methods to treat fly ash, e.g., the extraction of heavy metals by acidic leaching. One new technology is FLUWA (washing of fly ash), which was developed in Switzerland [11,12]. This method removes most heavy metals from fly ash efficiently. However, with this process, soluble salt components are also concentrated in the solution. The result is a heavy-metal-enriched saline solution. The typical treatment of the solution with lime milk causes the precipitation of the heavy metals as salt-rich hydroxides. Recovery of the heavy metals from these sludges is restricted due to the high concentration of Cl in the residues that leads to increased corrosion of the facilities. As a consequence, these sludges are usually disposed of. Therefore, the concentration of Cl in the residues needs to be reduced for an economic recoverability of these metals.

A new proposition is to use FLUREC (fly ash recycling), a hydrometallurgical process to recover Zn [11,13]. First, Pb, Cd, and Cu are removed by cementation using Zn-powder as a reducing agent. Second, Zn is transferred into an organic phase by solvent extraction. After re-extraction with sulfuric acid, Zn is in aqueous solution again and then recovered by electrolysis.

The recovery of heavy metals as a secondary resource from waste streams, such as FA from solid waste incineration, is therefore a challenging task. Is it possible to recover Zn in a simple way and at a low energy and low cost from wastewater as a valuable product? What influence does Pb have on the system? What are the consequences of a saline solution on the reaction products? These questions are the subject of this study.

A solution could be the “specific product-oriented precipitation” (SPOP) of heavy metals, based on a modified ferrite process. With this novel concept, it is possible to control the formation of phases directly by adjusting parameters such as concentration, temperature, pH, and Fe-addition. SPOP was developed in model systems and successfully applied to industrial wastewater containing Cu, Ni, Mn, Pb, Sn, Pd, Ag, and Au [14–18]. John et al. [19] succeeded in recovering Zn almost as a single phase in the form of nanocrystalline ZnO particles without adding Fe. Depending on the experimental parameters, at optimum conditions, removal efficiencies of 99.99% were realized for Zn. However, the influence of Pb and salinity on the precipitation of the product phases of Zn has not been investigated thus far. Herein, we present a study exploring the formation and dissolution of minerals in a model system by varying the experimental conditions on a laboratory scale. We prepared synthetic aqueous solutions (AQs), similar to wastewater from FLUWA at the municipal solid waste incineration (MSWI) plant in Ingolstadt, Germany, to study the effect of Pb and salinity on water purification and precipitation product.

2. Materials and Methods

2.1. Material

Table 1 shows the concentration of the main components, Zn, Pb, Na, K, Ca, SO_4 , and Cl, of four “leachate wastewater” samples (WW1 to WW4) after leaching fly ash with the FLUWA process from the MSWI plant in Ingolstadt, Germany. The concentrations of the components vary significantly, e.g.,

the fluctuation of Zn ranges between 711 and 3570 mg/L, which means variability by a factor of ~5. The concentration of Cl is almost constant between samples, varying by a factor of ~1.2.

Table 1. Composition of the four leachate wastewater (WW) samples from the municipal solid waste incineration (MSWI) plant Ingolstadt (n.d. = not determined).

Element	WW1 (mg/L)	WW2 (mg/L)	WW3 (mg/L)	WW4 (mg/L)
Zn	3570	1650	711	2600
Pb	1780	204	70	970
Na	32,200	22,500	n.d.	27,900
K	6730	7780	n.d.	4580
Ca	4340	3450	n.d.	7880
SO ₄	2400	3000	1400	1900
Cl	71,000	60,000	69,000	71,000

2.2. Experimental Series

• Purpose and Scope

To keep the model system simple and still realistic, we prepared a synthetic aqueous solution to exclude effects caused by accessory elements, impurities, or organic matter. The composition of our synthetic AQ is based on WW1 (see Table 1). Our focus in this study is on precipitation experiments with Zn-containing synthetic AQ with differing salinity and Pb concentration. The concentration of Zn was always 2000 mg/L. Three different sets of experiments were performed to study the influence of Pb and salinity on the precipitation of Zn.

• Nomenclature

The nomenclature used is as follows: the first part represents the main element Zn. The second, where necessary, indicates the concentration of Pb relative to Zn (cast as a percentage). The last part of the nomenclature denotes the AQ of the experiment: “high” for the high saline, “med” for the medium saline, and “low” for the low saline solution. E.g., Zn₁₀Pb_{low} denotes the experiment with 2000 mg/L Zn and 10% Pb (200 mg/L) in low saline solution.

• Influence of Salinity

Two experimental sets were conducted to investigate the influence of salinity. Table 2 summarizes the composition of the AQ in the Zn system (exp. set 1) and the Zn–Pb system (exp. set 2). In the first set, the “Zn system”, the impact of salinity on Zn precipitation was studied. Aqueous solutions with three different compositions were applied: a low saline, a medium saline, and a high saline AQ.

In the second experiment set, the “Zn–Pb system”, the influence of Pb on the precipitation of Zn in the three different AQS was tested. Therefore, 200 mg/L Pb was added (10% Pb of Zn concentration). The “low saline” solution in the Zn and Zn–Pb systems contains about 0 to 3000 mg/L sulfate and chlorine. Concentrations in “medium saline” solutions vary between 7000 and 9200 mg/L chlorine and 250 to 3150 mg/L sulfate. “High saline” AQS contain $\geq 70,000$ mg/L chlorine and ≥ 2500 mg/L sulfate.

Table 2. Composition of the aqueous solutions (AQS) in the Zn System (exp. set 1) and the Zn–Pb System (exp. set 2).

Set	System	Experiment	Zn (mg/L)	Pb (mg/L)	Na (mg/L)	K (mg/L)	Ca (mg/L)	SO ₄ (mg/L)	Cl (mg/L)					
1	Zn	Zn _{low}	2000	0	3000	700	400	2900	0					
		Zn _{med}								3150	7000			
		Zn _{high}								5400	70,000			
2	Zn–Pb	Zn ₁₀ Pb _{low}	2000	200	3000	700	400	250	9200					
		Zn ₁₀ Pb _{med}								30,000	7000	4000	2500	72,200
		Zn ₁₀ Pb _{high}												

- Influence of Pb

Table 3 shows the composition of the AQ in the Zn–Pb–salt system (exp. set 3). The aim here was to study the impact of Pb variation on the precipitation of Zn. The AQ in the “Zn–Pb–salt system” was always high saline and the Pb-concentration was varied from 100 to 800 mg/L.

Table 3. Composition of the aqueous solutions in the Zn–Pb–salt System (exp. set 3).

Set	System	Experiment	Zn (mg/L)	Pb (mg/L)	Na (mg/L)	K (mg/L)	Ca (mg/L)	SO ₄ (mg/L)	Cl (mg/L)
3	Zn–Pb–salt	Zn_5Pb_high	2000	100	30,000	7000	4000	2500	72,200
		Zn_10Pb_high		200					72,240
		Zn_40Pb_high		800					72,440

2.3. Experimental Setup

For the preparation of the saline AQS, NaCl (VWR, Darmstadt, Germany, analytical grade), HCl (32%), KCl, CaCl₂·2H₂O, CaSO₄·2H₂O, PbCl₂, ZnCl₂, and ZnSO₄·7H₂O (Merck, Darmstadt, Germany, analytical grade) were used. The volume used for the experiments was 250 mL.

The synthetic solution was heated up to a reaction temperature of 30 °C for the Zn system (exp. set 1) and 40 °C for both the Zn–Pb (exp. set 2) and Zn–Pb–salt (exp. set 3) systems. Subsequently, the solution was alkalized with NaOH to pH >9 and the pH value was kept constant at pH ≥9 for a minimum of 5 min to ensure a homogeneous solution. The solution was stirred during the whole experiment. For monitoring temperature and adjusting pH, an automatic titration unit, Titrator TL 7000 from SI Analytics (Xylem Analytics Germany, Weilheim, Germany), was used.

After precipitation, the suspension was filtered. One part of the residues was washed with pure water (<2 μS/cm) to remove water-soluble salts, the other part remained untreated, and both parts were dried at room temperature for at least 24 h. The filtrate was kept for further analysis.

2.4. Methods

The concentration of the cations in the wastewater was determined by an ICP-OES, type Optima 2000 DV from Perkin Elmer by the Bavarian Environment Agency (Augsburg, Germany). The chemistry after the experiments was determined by ICP-MS, type 7500 from Agilent Technologies by the Stadtwerke München (Munich, Germany).

The concentrations of Cl[−] and SO₄^{2−} in the solutions were measured by ion chromatography (IC) according to DIN EN ISO 10304-1 [20]. It was performed either by Analytik Institut Rietzler GmbH (Nuremberg, Germany), or by the Bavarian Environment Agency (Augsburg, Germany).

Phase identification was achieved using X-ray powder diffraction (XRD) with a GE diffractometer, XRD 3003 TT of the Department of Earth and Environmental Sciences (DEES), Ludwig-Maximilians-Universität (LMU) München, operated at 30 kV and 40 mA with a primary monochromator. The data was collected using Cu Kα₁ radiation. Phase identification was performed qualitatively by comparing the XRD patterns with the Inorganic Crystal Structure Database (ICSD) [21] and the Crystallography Open Database (COD) [22–26].

To identify low crystallinity phases, Fourier transform infrared spectroscopy (FTIR) was used. All spectra were recorded on an EQUINOX55 from Bruker at DEES, LMU München. The raw spectra were corrected for atmospheric interferences and for baseline, and the absorption bands were fitted using the software Peakfit. The profiles were compared with files of the database RRUFF [27] and with additional literature.

3. Results

3.1. Water Purification

Table 4 shows a summary of the heavy metal concentrations in the filtrates after the experiments. The calculated removal efficiency of ions reflects the recovery of the heavy metals from the solution. Thus, a high removal efficiency means that the metals are enriched in the precipitates.

Table 4. Concentration (mg/L) and removal efficiency (%) of Pb and Zn after the experiments.

Exp. Set	Experiment	Conc. Zn (mg/L)	Removal Efficiency of Zn (%)	Conc. Pb (mg/L)	Removal Efficiency of Pb (%)
1	Zn_low	≤0.05	>99.99	-	-
	Zn_med	0.60	99.97	-	-
	Zn_high	3.20	99.84	-	-
2	Zn_10Pb_low	81.24	95.94	6.48	96.76
	Zn_10Pb_med	0.30	99.98	0.29	99.85
	Zn_10Pb_high	1.22	99.94	0.8	99.60
3	Zn_5Pb_high	1.17	99.94	0.74	99.26
	Zn_10Pb_high	1.22	99.94	0.80	99.6
	Zn_40Pb_high	1.23	99.94	0.86	99.89

- Influence of Salinity on the Precipitation of Zn in the Zn System (Exp. Set 1) and the Zn-Pb System (Exp. Set 2)

Figure 1 gives an overview of the removal efficiency of Zn and Pb in the Zn system and the Zn-Pb system. In the Zn system (exp. set 1), the removal efficiency achieved in the experiment with low saline AQ was better than 99.9%. With increasing salinity, the removal efficiency for Zn decreased, even though it remained always >99.8%. After the experiment with high saline solution, the concentration of Zn was 3.2 mg/L (see Table 4).

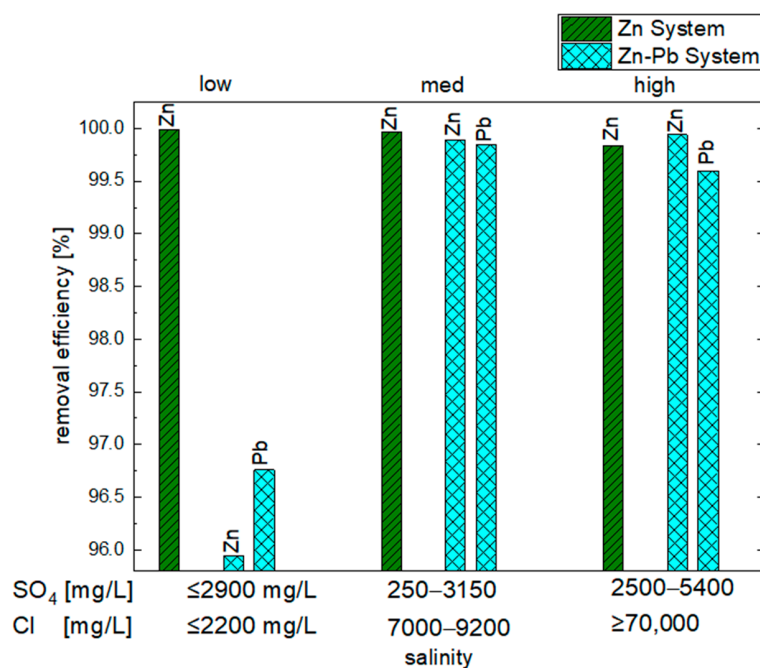


Figure 1. Removal efficiency of Zn and Pb in dependence of salinity in the Zn system (exp. set 1) and the Zn-Pb system (exp. set 2).

In the Zn–Pb system (exp. set 2) with 10% Pb added to the Zn-containing AQ, a different effect was observed (see Figure 1). The experiment with low saline AQ shows the lowest removal efficiency of 95.9% for Zn and 96.8% for Pb. The best results were obtained in the experiment Zn_10Pb_medium performed with medium saline solution. After the experiment, >99.9% Zn and 99.8% Pb were removed. In high saline solution, however, the removal efficiency decreased again for both Zn and Pb, even though the result was better than in the experiment with low saline AQ. In comparison with the Zn system, the removal efficiency was even slightly better. After precipitation, the concentration of chlorine in AQ did not change with increasing salinity, whereas the concentration of sulfate decreased.

- Influence of Pb in the Zn–Pb–Salt System (Exp. Set 3)

In experiment set 3, the effect of varying Pb concentration from 5% to 40% relative to Zn (2000 mg/L) in a high saline solution was studied (see Table 4). As shown in Figure 2, variation of Pb did not have an impact on the removal efficiency of Zn (99.9%). With increasing Pb-content in the high saline solution, the removal efficiency of Pb increased from 99.3% to 99.9%.

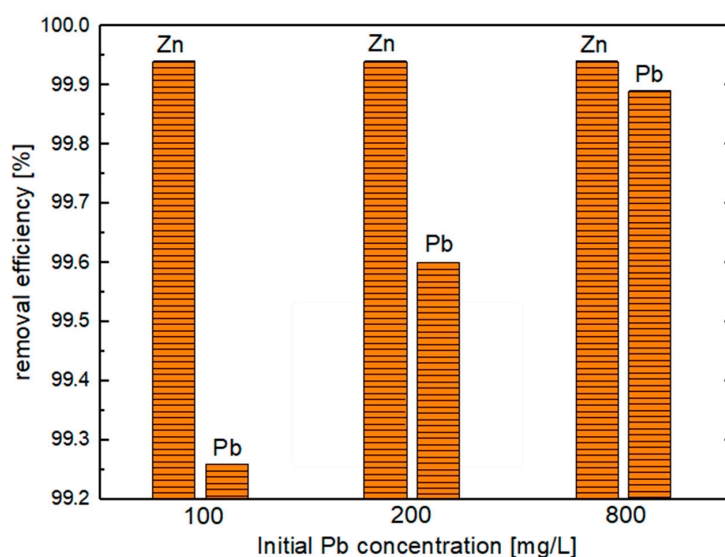


Figure 2. The dependence of Pb concentration on the removal efficiency in the Zn–Pb–salt System (exp. set 3).

3.2. Mineralogical Characterization

In order to assign and verify the phases in XRD and FTIR spectroscopy, we considered various literature dealing with possible Pb and Zn compounds, such as phases observed in specific locations such as Laurion, Greece [28], investigated for crystal structure and chemistry (e.g., [29–32]), or found as corrosion products (e.g., [33]).

3.2.1. Influence of Salinity

- Zn System (Exp. Set 1)

Figure 3 shows the change in XRD pattern of the washed precipitates in the Zn system. The XRD patterns show that the salinity of the solution has an impact on the precipitated phases. The main phase in the experiment with low saline AQ was zincite (ZnO) with sharp peaks at $31.94^\circ 2\theta$, $34.44^\circ 2\theta$, and $36.27^\circ 2\theta$ and related minor peaks. At $8.53^\circ 2\theta$, there was a broad peak that matches to the main reflex of namuwite ($\text{Zn}_4(\text{SO}_4)(\text{OH})_6 \cdot 4\text{H}_2\text{O}$). A sharp peak with low intensity at $11.78^\circ 2\theta$ corresponds to bechererite with the general formula $(\text{Zn,Cu})_6\text{Zn}_2(\text{OH})_{13}[(\text{S,Si})(\text{O},\text{OH})_4]_2$; the additional minor peaks were also observed.

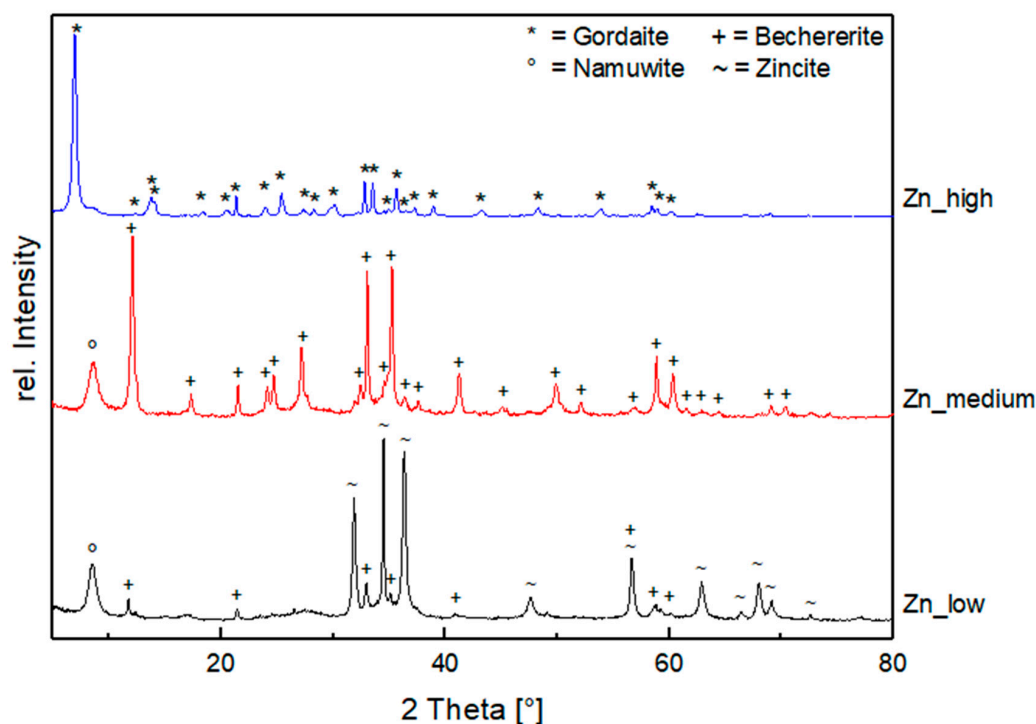


Figure 3. XRD pattern ($\text{Cu K}\alpha_1$) of the washed precipitates in the Zn system (exp. set 1) with increasing salt content in the aqueous solution.

Zincite was not detected in the experiment with medium saline AQ Zn medium. The main phase was bechererite in addition to a minor amount of namuwite. As shown in Figure 3, compared to experiment Zn_low, performed with low saline AQ, the intensity of the bechererite reflexes are significantly higher.

With increasing salinity, the concentration of chloride and sulfate increased in the precipitate. The main phase in the experiment with high saline AQ was gordaite ($\text{NaZn}_4(\text{SO}_4)(\text{OH})_6\text{Cl}\cdot 6\text{H}_2\text{O}$) with a main peak at $6.84^\circ 2\theta$. A broad peak with low intensity next to the main reflex of gordaite indicates the main peak of namuwite. No other phases were detected in the XRD pattern of the washed precipitate Zn high.

- Zn–Pb System (Exp. Set 2)

Figure 4 shows the XRD pattern of the washed precipitates with increasing salt content in the Zn–Pb system. The main phase in the experiment with low saline AQ is zincite. In comparison, the experiment with medium saline AQ shows lower overall intensities with broad peaks of bechererite and a differing proportion of zincite main peaks. Small peaks at 24.68° and $27.11^\circ 2\theta$ could not be assigned to any known phase. In contrast to the Zn system (exp. set 1; Figure 3), namuwite was not detected in the experiments with low or medium saline AQ. A change in intensity of the zincite main peaks was also observed.

In the salt-rich experiment Zn₁₀Pb_{high} (exp. set 3), gordaite was the main phase (see Figure 4). A broad peak with low intensity next to the main peak of gordaite indicates small amounts of namuwite. Other phases were not observed. In all three experiments with 10% Pb, no Pb-bearing phase was detected, either in the XRD patterns or in the FTIR spectra.

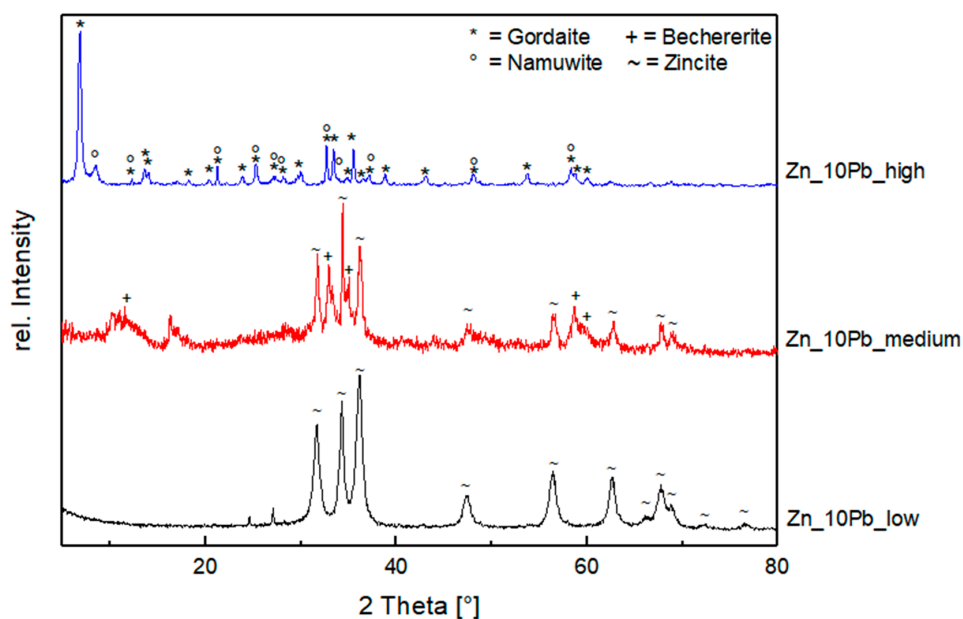


Figure 4. XRD pattern ($\text{Cu K}\alpha_1$) of the washed precipitates in the Zn/Pb-model system (exp. set 2) with increasing salt content in the AQ.

3.2.2. Influence of Pb in High Saline Solution (Exp. Set 3)

Figure 5 shows the effect of a Pb ratio between 5% and 40% on the XRD pattern of the washed precipitates in the Zn–Pb–salt system with high saline AQ. The XRD patterns of all experiments are very similar. The reflexes match to gordaite as the main phase. Starting with a concentration of 10% Pb in the solution, a broad peak appears next to the main peak of gordaite, matching the (001) reflex of namuwite. When 40% Pb was added, the relative intensity of this reflex decreased. Additional reflexes occurring in the XRD pattern match laurionite ($\text{Pb}(\text{OH})\text{Cl}$) with main peaks at 22.15° 2θ (210), 27.06° 2θ (111), and 35.49° 2θ (301).

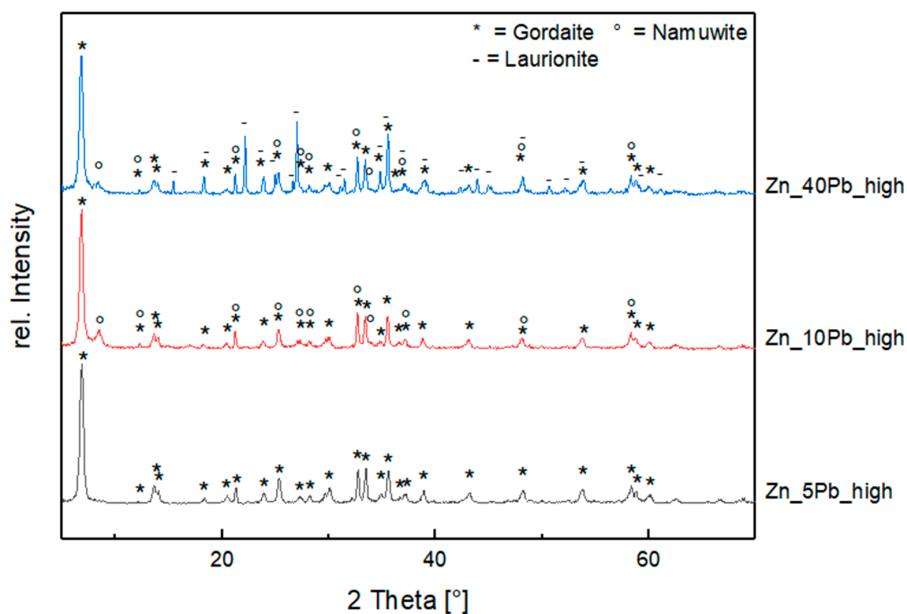


Figure 5. XRD pattern ($\text{Cu K}\alpha_1$) of the washed precipitates in the Zn–Pb–salt system (exp. set 3) with increasing Pb content in high saline solution.

Figure 6 shows the FTIR spectra of the washed precipitates from experiments with varying Pb concentration in high saline AQ (exp. set 3). The variation of Pb from 5% to 40% shows only slight effects. The relative intensity of the bands of namuwite at 1158 cm^{-1} and 1387 cm^{-1} increased slightly with increasing Pb concentration. This effect is observable at 390 cm^{-1} , too. Bands of laurionite show no change in their intensity and are always present. Bechererite bands show a slight decrease at 815 cm^{-1} . A shift of the bands with increasing Pb content was not observed.

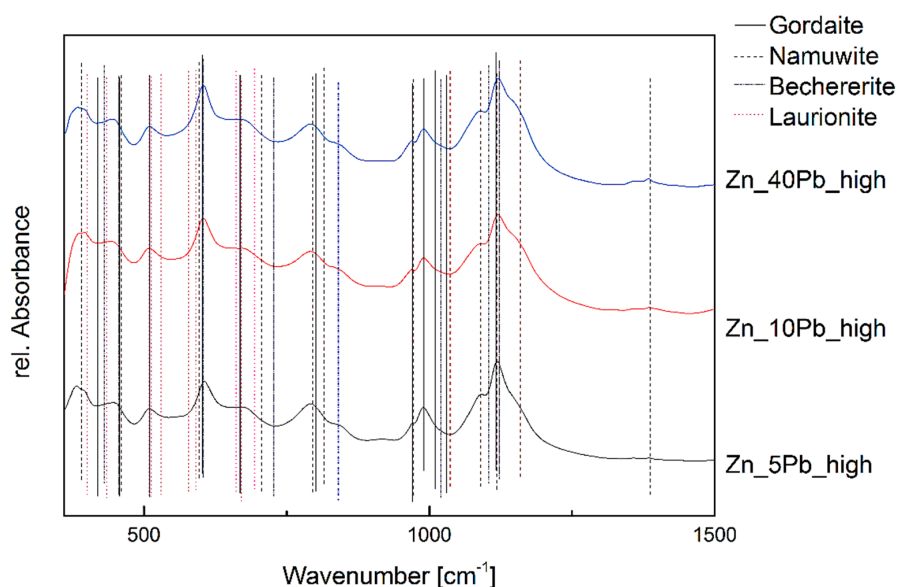


Figure 6. Fingerprint area of the IR Spectra of the washed precipitates in the Zn–Pb–salt system (exp. set 3) with varying Pb content.

3.2.3. Washing of the Precipitates

One part of the precipitates was always washed before mineralogical characterization to remove water-soluble salts, such as halite; the other part was left as is. In the experiments with low saline AQ, no change of the XRD patterns was observed. However, after washing the precipitates obtained from AQ with medium and high salinity, the X-ray patterns differ.

- Zn System (Exp. Set 1)

Figure 7 shows the XRD diffraction pattern of the washed (w) and unwashed (uw) precipitates of experiment Zn_medium. The XRD pattern of the unwashed sample exposes sharp peaks of gordaite as the main phase and minor peaks of bechererite. After washing the precipitate, the diffractogram in the experiment with medium salinity in AQ differed considerably. Bechererite occurred as the main phase together with smaller, broad peaks assigned to namuwite. Gordaite was no longer detected.

- Zn–Pb System (Exp. Set 2)

In the experiment with 10% Pb added to AQ, the main phases of the unwashed samples were halite and gordaite together with a small amount of zincite and traces of bechererite. After washing the precipitate, halite and gordaite were no longer present, and zincite and broad peaks of bechererite were observed.

- Zn–Pb–Salt System (Exp. Set 3)

No significant change in the phases was observed in the experiments with high saline AQ and varying Pb content. After washing the residue, the intensity of the gordaite peaks slightly decreased and that of namuwite increased.

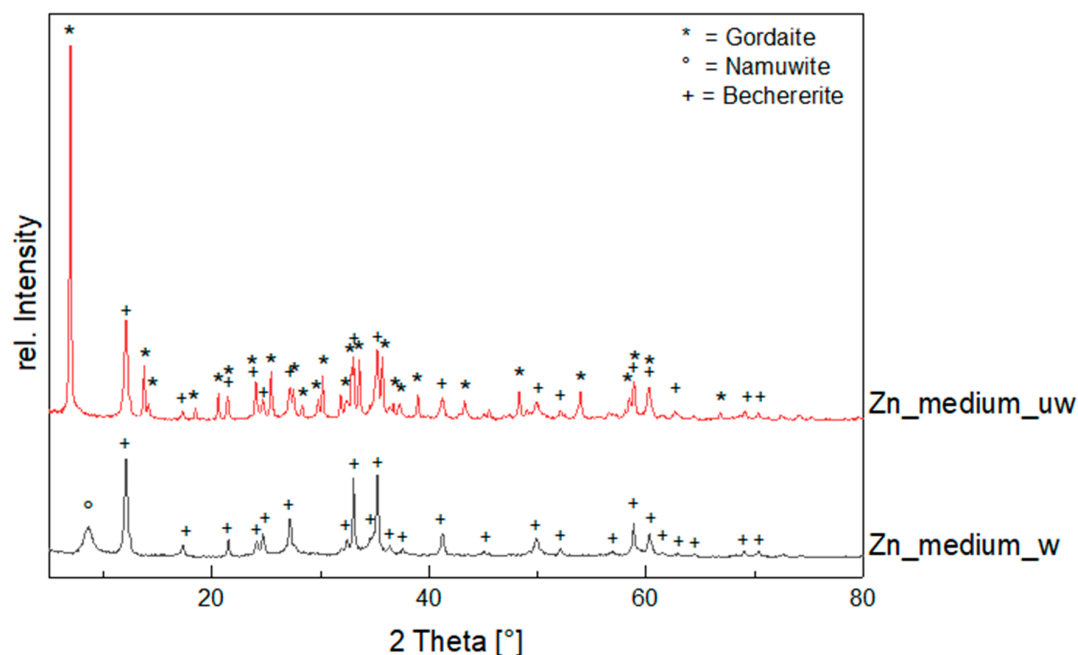


Figure 7. XRD pattern (Cu K α_1) of the washed (w) and unwashed (uw) precipitates of experiment Zn medium (exp. set 1).

4. Discussion

4.1. Influence of Salinity

Figure 8 gives an overview of the experimental results. The increasing salinity in the AQ promotes the formation of phases with higher sulphate, chlorine, and hydroxide in the structure. The various types of Zn sulphate hydroxides reflect an increasing incorporation of Cl and SO₄ in the residue.

		salinity in AQ			
		low	medium	high	
Zn-content in residue	Zincit	+++	-	-	Zn System
	ZnO	+++	+	-	Zn-Pb System
	Bechererite	(+)	+++	-	Zn System
	Zn₆Zn₂(OH)₁₃(SO₄)₂	-	(+)	-	Zn-Pb System
	Namuwite	+	+	-	Zn System
	Zn₄(SO₄)(OH)₆·4H₂O	-	-	(+)	Zn-Pb System
	Gordaite	-	-	+++	Zn System
	NaZn₄(SO₄)(OH)₆Cl·6H₂O	-	-	+++	Zn-Pb System

Figure 8. Crystalline phases in the Zn system (exp. set 1) and the Zn–Pb system (exp. set 2) as a function of the salinity in the AQ (the number of + equals the relative amount of the phase in the residue, (+) indicates traces of the phase, - means phase not present).

In the Zn system (exp. set 1), zincite is only formed in low saline AQ together with low amounts of Zn-sulfate-phase namuwite. The high recovery rate >99.9% for low saline AQ is in accordance with John et al. [19]. At optimum conditions, the authors obtained mainly zincite nanoparticles, and noticed that the amount of co-precipitated phases, smithsonite (ZnCO_3) and zinc hydroxide ($\text{Zn}(\text{OH})_2$), was below the detection limit of XRD. The occurrence of namuwite and the lack of smithsonite or zinc hydroxide in our experiment Zn low is most probably due to the differing AQ composition. With increasing salinity, at medium concentrations (7000 to 9200 mg/L chlorine, 250 to 3150 mg/L sulfate) zincite is replaced by bechererite whereas namuwite is still present. An absence of Cu and Si does not limit the formation of bechererite; it solely effects the chemistry of the solid solution. The broad profile of the namuwite peaks indicates that this phase has low crystallinity [34]. At high salinity ($\geq 70,000$ mg/L Cl), gordaite preferentially grows, which means an additional incorporation of Na, Cl, and water into the crystal structure.

The addition of 10% Pb to the AQ in the Zn–Pb system (exp. set 2) has a strong impact on the stability of zincite (see Figure 1, Figure 4, and Figure 8). The lower Zn removal efficiency observed in the presence of Pb at low salinity indicates that Pb inhibits the precipitation of zincite. However, the presence of zincite at medium salinity means that the stability field of zincite can be enlarged significantly by adding Pb. The changing intensity of the three main peaks of ZnO in low and medium AQs is a strong indication for a changed morphology of the ZnO particles [19,35]. In the presence of foreign atoms, the preferential growth of the ZnO nanostructure can be modified [36]. Furthermore, the low intensity of the reflexes in medium saline AQ is interpreted as a decrease of the crystallinity or size of the phases. Changes in the crystal structure (atomic positions, occupancy, and texture) of the precipitates may also lead to a decrease of their intensity with respect to the background [34,37]. A lower content of bechererite at intermediate salt contents compared to the Zn system is obviously effected by the larger stability field of zincite. In contrast to the Zn system, the presence of Pb in the solution shifts the stability field of namuwite to higher Cl-concentrations. Gordaite is the stable phase in the high saline AQ independently of the Pb-concentration (see Figure 8).

4.2. Influence of Pb (Exp. Set 3)

Figure 9 displays the formation of crystalline phases with varying Pb concentration. The experiments in the high saline Zn–Pb–salt system show that Pb has no impact on the removal efficiency of Zn. Furthermore, the removal efficiency of Pb increases with higher Pb concentration in the solution, even though Pb-containing phases were only detected at 40% Pb by XRD. The occurrence of laurionite at <40% Pb in AQ implies that a sufficiently high concentration of Pb in the solution is necessary to form a distinct Pb-containing phase that can be detected via XRD. The very similar IR spectra of the three experiments in Figure 6 shows that almost all bands of gordaite, namuwite, bechererite, and laurionite are superimposed. Therefore, it also seems possible that laurionite is already present at lower Pb concentrations <40%, but is not detected because the content lies below the detection limit of XRD, which is approximately at 3 wt %. These results correspond very well with observations in natural environments, as laurionite is only observed in the presence of salt in rocks. Regenspurg et al. [38] identified laurionite in highly saline geothermal fluids from a Permian Rotliegend reservoir. They concluded that the formation of Pb-hydroxychloride is favored at pH values above 7.2 and low temperatures [38].

Another possible explanation for the improved removal efficiency of Pb is its incorporation in the structure of the mineral phases, such as gordaite, bechererite, or namuwite. Ion exchanges should be detectable with XRD or FTIR because of the differing size of the ions. However, we observed no shift in the position of the reflexes in XRD or bands in the FTIR pattern. The minor changes in intensity of the (001) reflex of namuwite in the experiment with 10% Pb point rather to changed stability fields of namuwite at the expense of bechererite.

In general, a substitution of Pb^{2+} by Zn^{2+} is not expected since compared to Zn^{2+} , the ionic radius of the Pb^{2+} ion in an octahedral environment is too large. However, all of these minerals—gordaite,

bechererite, and namuwite—have a sheet structure with hydrogen bonds between the layers, which allows for a higher flexibility of the structure. Thus, ions such as Pb^{2+} can substitute vacancies and may replace Zn^{2+} in the structure. Maruyama et al. [39] synthesized gordaite and studied the exchange capacity with Ca, K, and Li. They concluded that gordaite has high potential as a cation exchanger layered hydroxide salt.

		Pb-content in solution [%]		
		5	10	40
 Zn-content in residue	Bechererite $\text{Zn}_6\text{Zn}_2(\text{OH})_{13}(\text{SO}_4)_2$	-	-	-
	Namuwite $\text{Zn}_4(\text{SO}_4)(\text{OH})_6 \cdot 4\text{H}_2\text{O}$	-	(+)	(+)
	Gordaite $\text{NaZn}_4(\text{SO}_4)(\text{OH})_6\text{Cl} \cdot 6\text{H}_2\text{O}$	+++	+++	+++
	Laurionite $\text{Pb}(\text{OH})\text{Cl}$	-	-	++

Figure 9. Crystalline phases in the Zn–Pb–salt system (exp. set 3) as a function of Pb concentration in the AQ (the number of + equals the relative amount of the phase in the residue, (+) indicates traces of the phase, - means phase not present).

4.3. Washing the Precipitates

A dependency between washing the precipitates and Pb concentrations could not be found. There is no change of intensity in the XRD patterns of laurionite. The same was observed for zincite; we could not find a difference in the XRD pattern of zincite after washing. However, the comparison of the washed and unwashed XRD patterns showed that the Cl-rich phases of gordaite and halite disappeared after washing with pure water. This effect is very reasonable for halite because of its high solubility in water. Gordaite, however, is not soluble in pure water. Maruyama et al. [38] also washed their precipitates after synthesis and the gordaite did not disappear. The comparison of the XRD pattern of the Zn_{medium} unwashed and washed (exp. set 1) residues showed no change for bechererite. However, the disappearance of gordaite after washing was accompanied by the occurrence of namuwite with broad peaks. The washed precipitates of both the Zn–Pb system (exp. set 2) and the Zn–Pb–salt system (exp. set 3) show the same trend; the only difference is the changed intensity of the phases, with the highest effect observed at medium salinity. The lower intensity observed in medium saline AQ is interpreted as a decrease in the crystallinity or size of the phases. Changes in the crystal structure (atomic positions, occupancy, and texture) of the precipitates may also lead to a decrease in their intensity [34,37].

According to Hawthorne and Sokolova [29], the structures of gordaite, namuwite, and bechererite are closely related as they all contain alternating sheets with octahedral and tetrahedral sites (homeomorphic to graph 4b of Hawthorne and Schindler [40]). Figure 10 shows the generic structure for gordaite and namuwite. Zn occurs mainly in the center of the tetrahedrons and partly in the center of the octahedrons. Bechererite has six octahedrally coordinated cations, and every seventh octahedron is vacant. Furthermore, two tetrahedrally coordinated Zn cations form a pyro-group leading to a very

ordered structure of this mineral phase [29]. Therefore, bechererite can be excluded as an exchange product of gordaite.

The sheet-like structures of Gordaite and namuwite consist of alternating sheets with tetrahedral and octahedral sites. In gordaite, Cl^- atoms (see Figure 10a, green) occupy the tip of the tetrahedron, resulting in a negative charge, which is balanced by incorporating Na^+ ions between the layers. The Na^+ ions are octahedrally coordinated, surrounded by six water molecules, and held by hydrogen bonds. This means that the intercalated Na^+ ions are weakly bonded between the sheets. The structure of namuwite is comparable; it has also the sequence tetrahedron–octahedron–tetrahedron, connected via hydrogen bonds; but in contrast with gordaite, it does not include Na^+ and Cl^- in the structure (see Figure 10b). Therefore, we suggest that washing the precipitate with pure water removes the Na^+ ions from the structure. Without the missing charge, Cl^- in the tetrahedrons of gordaite is substituted by OH^- . Rearrangement of the structure leads to the formation of low crystalline namuwite. Our results show that, even at high salinity in the AQ, gordaite may be transferred to namuwite. After washing with pure water, the intensity of gordaite reflexes slightly decreased, whereas that of namuwite increased. This trend is in agreement with Maruyama et al. [39]. They detected small amounts of osakaite ($\text{Zn}_4(\text{SO}_4)(\text{OH})_6 \cdot 5\text{H}_2\text{O}$) in their synthesized residue. Drying at room temperature on air can lead to Namuwite, a partially dehydrated derivative of osakaite.

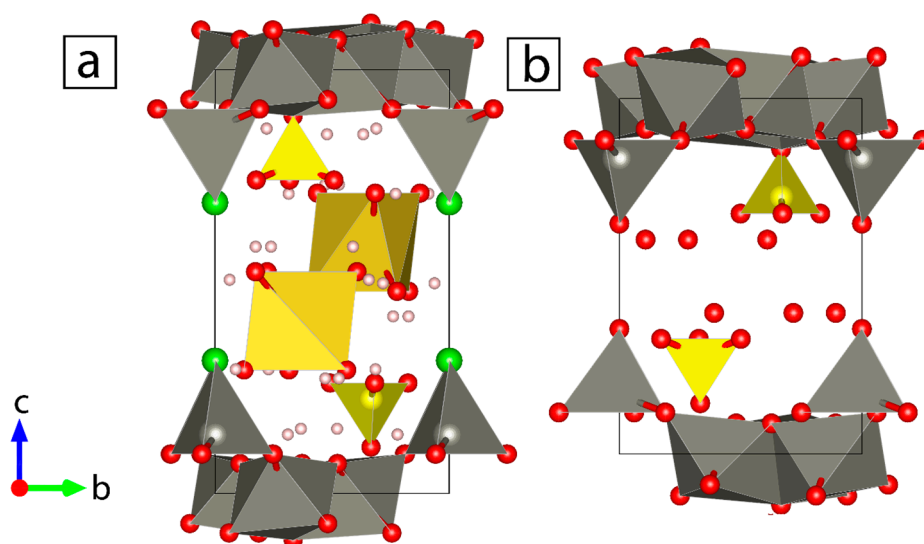


Figure 10. Structure of (a) gordaite (after [30]) and (b) namuwite (after [31]) along the *c*-axis (red atoms = O, green atoms = Cl, center of yellow tetrahedrons = S, center of yellow octahedrons = Na; crystal structures were created with the software VESTA).

5. Conclusions and Outlook

Our investigations in low, medium, and high saline Zn–Pb systems clearly show that the formation of the mineral phases depends sensitively on the environmental conditions. Low salinity can lead to formation of zincite depending on the experimental parameters. Addition of 10% Pb to medium saline AQ enlarges the stability field of zincite but reduces the recovery of Zn and leads to low crystallinity of the precipitates. High salinity (>70,000 mg/L Cl; >2500 mg/L SO_4) results always in gordaite as the main phase, whereas at medium salinity (7000 to 9200 mg/L Cl; 250 to 3150 mg/L SO_4), bechererite precipitates as the main phase. The formation of laurionite, a Pb-hydroxychloride, seems to be favored at high salinity. Our results show that the limiting factor for gordaite stability is the Cl concentration: it is only stable at high Cl-concentrations. At Cl-concentrations ≤ 9200 mg/L, gordaite becomes metastable and is transformed to namuwite.

The study was performed in a simplified model system, to exclude effects caused by accessory elements, impurities, or organic matter. Preliminary results with leachate wastewater from MSWI fly ash show similar trends. Accordingly, the findings of our study can be used to improve the extraction process. Formation of the phase namuwite and bechererite is beneficial because of the higher Zn content and lower amount of water in the crystal structure. The observed transformation of gordaite to namuwite by washing the precipitates can actively be used to enrich Zn in the residues and helps to reduce Cl-concentration in the precipitates. In contrast to precipitation with lime milk, treating leachate wastewater from MSWI fly ash with the optimized SPOP process can produce residues with high potential for recycling. The lower Cl-content, the higher concentration of Zn, and the lower amount of water in the residues are beneficial for smelting.

Acknowledgments: This study was funded by MSWI plant Ingolstadt, Germany, and partly funded by the Bavarian State Ministry of the Environment and Consumer Protection. The authors want to thank Jürgen Diemer from the Bavarian Environment Agency and Ottmar Hofmann from the Stadtwerke München for the analytical support. Thanks also to Gerhard Meier and Michael Funk, MSWI plant Ingolstadt, for providing information and discussion. Additionally, we like to thank Ana Sylvia Casas Ramos, Adriana Gerz, Martina Oberreit, and Christian Obermeier for performing the water analysis.

Author Contributions: Kai Tandon and Melanie John conceived and designed the experiments; Valentin Schaller performed the experiments, part of which formed his Bachelors Thesis; Kai Tandon and Valentin Schaller conducted the mineralogical and chemical analysis; Kai Tandon, Soraya Heuss-Aßbichler, Melanie John, and Valentin Schaller discussed and interpreted the data; Kai Tandon wrote the paper.

Conflicts of Interest: The authors declare no conflict of interest. The founding sponsors had no role in the design of the study; in the collection, analyses, or interpretation of data; in the writing of the manuscript, and in the decision to publish the results.

References

1. Nordberg, G.F.; Fowler, B.A.; Nordberg, M. *Handbook on the Toxicology of Metals*, 4th ed.; Academic Press: Cambridge, MA, USA, 2014.
2. Zepf, V.; Simmons, J.; Reller, A.; Ashfield, M.; Rennie, C. *Materials Critical to the Energy Industry: An Introduction*; BP p.l.c.: London, UK, 2014.
3. Gidlow, D. Lead toxicity. *Occup. Med.* **2004**, *54*, 76–81. [[CrossRef](#)]
4. Fu, F.; Wang, Q. Removal of heavy metal ions from wastewater: A review. *J. Environ. Manag.* **2011**, *92*, 407–418. [[CrossRef](#)] [[PubMed](#)]
5. Naja, G.M.; Volesky, B. Treatment of Metal-Bearing Effluents: Removal and Recovery. In *Heavy Metals in the Environment*; Wang, L.K., Chen, J.P., Hung, Y.-T., Shammass, N.K., Eds.; CRC Press: Boca Raton, FL, USA, 2009; p. 247.
6. Youcai, Z. *Pollution Control and Resource Recovery: Municipal Solid Wastes Incineration: Bottom Ash and Fly Ash*; Butterworth-Heinemann: Oxford, UK, 2016.
7. Tang, J.; Steenari, B.-M. Leaching optimization of municipal solid waste incineration ash for resource recovery: A case study of Cu, Zn, Pb and Cd. *Waste Manag.* **2016**, *48*, 315–322. [[CrossRef](#)] [[PubMed](#)]
8. Zacco, A.; Borgese, L.; Gianoncelli, A.; Struis, R.P.; Depero, L.E.; Bontempi, E. Review of fly ash inertisation treatments and recycling. *Environ. Chem. Lett.* **2014**, *12*, 153–175. [[CrossRef](#)]
9. Wang, K.-S.; Chiang, K.-Y.; Lin, S.-M.; Tsai, C.-C.; Sun, C.-J. Effects of chlorides on emissions of toxic compounds in waste incineration: Study on partitioning characteristics of heavy metal. *Chemosphere* **1999**, *38*, 1833–1849. [[CrossRef](#)]
10. Li, J.-S.; Xue, Q.; Wang, P.; Wang, H.-Q.; Zhang, T.-T. Leaching characteristics of chlorine from municipal solid waste incineration fly ash by up-flow percolation column tests. *Environ. Earth Sci.* **2016**, *75*, 31. [[CrossRef](#)]
11. Schlumberger, S.; Schuster, M.; Ringmann, S.; Koralewska, R. Recovery of high purity zinc from filter ash produced during the thermal treatment of waste and inerting of residual materials. *Waste Manag. Res.* **2007**, *25*, 547–555. [[CrossRef](#)] [[PubMed](#)]
12. Weibel, G.; Eggenberger, U.; Schlumberger, S.; Mäder, U.K. Chemical associations and mobilization of heavy metals in fly ash from municipal solid waste incineration. *Waste Manag.* **2017**, *62*, 147–159. [[CrossRef](#)] [[PubMed](#)]

13. Schlumberger, S.; Bühler, J. Metallrückgewinnung aus Filterstäuben der thermischen Abfallbehandlung nach dem FLUREC-Verfahren. In *Flaschen–Schlacken–Stäube–aus Abfallverbrennung und Metallurgie*; TK Verlag Karl Thomé-Kozmiensky: Neuruppin, Germany, 2013; pp. 377–398.
14. Heuss-Aßbichler, S.; John, M.; Klapper, D.; Bläß, U.W.; Kochetov, G. Recovery of copper as zero-valent phase and/or copper oxide nanoparticles from wastewater by ferritization. *J. Environ. Manag.* **2016**, *181*, 1–7. [[CrossRef](#)] [[PubMed](#)]
15. John, M.; Heuss-Aßbichler, S.; Park, S.-H.; Ullrich, A.; Benka, G.; Petersen, N.; Rettenwander, D.; Horn, S.R. Low-temperature synthesis of CuFeO₂ (delafossite) at 70 °C: A new process solely by precipitation and ageing. *J. Solid State Chem.* **2016**, *233*, 390–396. [[CrossRef](#)]
16. John, M.; Heuss-Aßbichler, S.; Ullrich, A. Conditions and mechanisms for the formation of nano-sized delafossite (CuFeO₂) at temperatures ≤ 90° C in aqueous solution. *J. Solid State Chem.* **2016**, *234*, 55–62. [[CrossRef](#)]
17. John, M.; Heuss-Aßbichler, S.; Ullrich, A.; Rettenwander, D. Purification of heavy metal loaded wastewater from electroplating industry under synthesis of delafossite (ABO₂) by “It-delafossite process”. *Water Res.* **2016**, *100*, 98–104. [[CrossRef](#)] [[PubMed](#)]
18. John, M.; Heuss-Aßbichler, S.; Tandon, K.; Ullrich, A. Recovery of Ag and Au from synthetic and industrial wastewater by 2-step ferritization and It-delafossite process via precipitation. *J. Water Process Eng.* **2017**. [[CrossRef](#)]
19. John, M.; Heuss-Aßbichler, S.; Ullrich, A. Recovery of Zn from wastewater of zinc plating industry by precipitation of doped ZnO nanoparticles. *Int. J. Environ. Sci. Technol.* **2016**, *13*, 2127–2134. [[CrossRef](#)]
20. *Water Quality—Determination of Dissolved Anions by Liquid Chromatography of Ions—Part 1: Determination of Bromide, Chloride, Fluoride, Nitrate, Nitrite, Phosphate and Sulfate*; ISO 10304-1:2007; German Version; ISO: Geneva, Switzerland, 2007.
21. Bergerhoff, G.; Brown, I.; Allen, F. Crystallographic databases. *Int. Union Crystallogr. Chester* **1987**, *360*, 77–95.
22. Downs, R.T.; Hall-Wallace, M. The American Mineralogist crystal structure database. *Am. Mineral.* **2003**, *88*, 247–250.
23. Gražulis, S.; Chateigner, D.; Downs, R.T.; Yokochi, A.; Quirós, M.; Lutterotti, L.; Manakova, E.; Butkus, J.; Moeck, P.; Le Bail, A. Crystallography open database—An open-access collection of crystal structures. *J. Appl. Crystallogr.* **2009**, *42*, 726–729. [[CrossRef](#)] [[PubMed](#)]
24. Gražulis, S.; Daškevič, A.; Merkys, A.; Chateigner, D.; Lutterotti, L.; Quiros, M.; Serebryanaya, N.R.; Moeck, P.; Downs, R.T.; Le Bail, A. Crystallography open database (COD): An open-access collection of crystal structures and platform for world-wide collaboration. *Nucleic Acids Res.* **2011**, *40*, D420–D427. [[CrossRef](#)] [[PubMed](#)]
25. Gražulis, S.; Merkys, A.; Vaitkus, A.; Okulič-Kazarinas, M. Computing stoichiometric molecular composition from crystal structures. *J. Appl. Crystallogr.* **2015**, *48*, 85–91. [[CrossRef](#)] [[PubMed](#)]
26. Merkys, A.; Vaitkus, A.; Butkus, J.; Okulič-Kazarinas, M.; Kairys, V.; Gražulis, S. COD: CIF: Parser: An error-correcting CIF parser for the perl language. *J. Appl. Crystallogr.* **2016**, *49*, 292–301. [[CrossRef](#)] [[PubMed](#)]
27. Lafuente, B.; Downs, R.T.; Yang, H.; Stone, N. The power of databases: The RRUFF project. In *Highlights in Mineralogical Crystallography*; Walter de Gruyter GmbH: Munich, Germany, 2016.
28. Gelaude, P.; van Kalmthout, P.; Rewitzer, C. *Laurion: The Minerals in the Ancient Slags*; Janssen Print: Nijmegen, Netherlands, 1996.
29. Hawthorne, F.C.; Sokolova, E. Simonkolleite, Zn₅(OH)₈Cl₂(H₂O), a decorated interrupted-sheet structure of the form [Mφ₂]₄. *Can. Mineral.* **2002**, *40*, 939–946. [[CrossRef](#)]
30. Adiwidjaja, G.; Friese, K.; Klaska, K.; Schlüter, J. The crystal structure of gordaite NaZn₄(SO₄)(OH)₆Cl·6H₂O. *Z. Krist.* **1997**, *212*, 704–707. [[CrossRef](#)]
31. Groat, L.A. The crystal structure of namuwite, a mineral with Zn in tetrahedral and octahedral coordination, and its relationship to the synthetic basic zinc sulfates. *Am. Mineral.* **1996**, *81*, 238–243. [[CrossRef](#)]
32. Hoffmann, C.; Armbruster, T.; Giester, G. Acentric structure (P3) of bechererite, Zn₇Cu(OH)₁₃[SiO(OH)₃SO₄]. *Am. Mineral.* **1997**, *82*, 1014–1018. [[CrossRef](#)]
33. Santana, J.; Fernández-Pérez, B.; Morales, J.; Vasconcelos, H.; Souto, R.; González, S. Characterization of the corrosion products formed on zinc in archipelagic subtropical environments. *Int. J. Electrochem. Sci.* **2012**, *7*, 12730–12741.
34. Le Bail, A. The profile of a Bragg reflection for extracting intensities. In *Powder Diffraction: Theory and Practice*; Dinnebier, R.E., Billinge, S.J., Eds.; RSC Publishing: Cambridge, UK, 2008; pp. 134–165.

35. Wu, C.; Qiao, X.; Chen, J.; Wang, H. Controllable ZnO morphology via simple template-free solution route. *Mater. Chem. Phys.* **2007**, *102*, 7–12. [[CrossRef](#)]
36. Abdelmohsen, A.H.; El Rouby, W.M.; Ismail, N.; Farghali, A.A. Morphology transition engineering of ZnO nanorods to nanoplatelets grafted Mo₈O₂₃–MoO₂ by polyoxometalates: Mechanism and possible applicability to other oxides. *Sci. Rep.* **2017**, *7*, 5946. [[CrossRef](#)] [[PubMed](#)]
37. Dinnebier, R.E.; Billinge, S.J. Principles of powder diffraction. In *Powder Diffraction: Theory and Practice*; Dinnebier, R.E., Billinge, S.J., Eds.; RSC Publishing: Cambridge, UK, 2008; pp. 1–19.
38. Regenspurg, S.; Feldbusch, E.; Byrne, J.; Deon, F.; Driba, D.L.; Hennings, J.; Kappler, A.; Naumann, R.; Reinsch, T.; Schubert, C. Mineral precipitation during production of geothermal fluid from a Permian Rotliegend reservoir. *Geothermics* **2015**, *54*, 122–135. [[CrossRef](#)]
39. Maruyama, S.A.; Krause, F.; Tavares Filho, S.R.; Leitão, A.A.; Wypych, F. Synthesis, cation exchange and dehydration/rehydration of sodium gordaite: NaZn₄(OH)₆(SO₄)Cl·6H₂O. *Appl. Clay Sci.* **2017**, *146*, 100–105. [[CrossRef](#)]
40. Hawthorne, F.C.; Schindler, M. Topological enumeration of decorated [Cu²⁺φ₂]_N sheets in hydroxy-hydrated copper-oxysalt minerals. *Can. Mineral.* **2000**, *38*, 751–761. [[CrossRef](#)]



© 2018 by the authors. Licensee MDPI, Basel, Switzerland. This article is an open access article distributed under the terms and conditions of the Creative Commons Attribution (CC BY) license (<http://creativecommons.org/licenses/by/4.0/>).